RESEARCH ARTICLE

FASEB BioAdvances   WILEY

The effects of *Tbx15* and *Pax1* on facial and other physical morphology in mice

Yu Qian[1,2,3] | Ziyi Xiong[4,5] | Yi Li[1,2,3] | Manfred Kayser[4] | Lei Liu[6] | Fan Liu[1,2,3,4]

[1]CAS Key Laboratory of Genomic and Precision Medicine, Beijing Institute of Genomics, Chinese Academy of Sciences, Beijing, China

[2]China National Center for Bioinformation, Beijing, China

[3]University of Chinese Academy of Sciences, Beijing, China

[4]Department of Genetic Identification, Erasmus MC University Medical Center Rotterdam, Rotterdam, the Netherlands

[5]Department of Epidemiology, Erasmus MC University Medical Center Rotterdam, Rotterdam, the Netherlands

[6]Department of Plastic and Burn Surgery, The Second Hospital, Cheeloo College of Medicine, Shandong University, Jinan, China

Correspondence
Fan Liu, Key Laboratory of Genomic and Precision Medicine, Beijing Institute of Genomics, Chinese Academy of Sciences, Beichen West Road 1-104, Chaoyang, Beijing, 100101, China.
Email: liufan@big.ac.cn.

Abstract

DNA variants in or close to the human *TBX15* and *PAX1* genes have been repeatedly associated with facial morphology in independent genome-wide association studies, while their functional roles in determining facial morphology remain to be understood. We generated *Tbx15* knockout ($Tbx15^{-/-}$) and *Pax1* knockout ($Pax1^{-/-}$) mice by applying the one-step CRISPR/Cas9 method. A total of 75 adult mice were used for subsequent phenotype analysis, including 38 *Tbx15* mice (10 homozygous $Tbx15^{-/-}$, 18 heterozygous $Tbx15^{+/-}$, 10 wild-type $Tbx15^{+/+}$ *WT* littermates) and 37 *Pax1* mice (12 homozygous $Pax1^{-/-}$, 15 heterozygous $Pax1^{+/-}$, 10 $Pax1^{+/+}$ *WT* littermates). Facial and other physical morphological phenotypes were obtained from three-dimensional (3D) images acquired with the HandySCAN BLACK scanner. Compared to *WT* littermates, the $Tbx15^{-/-}$ mutant mice had significantly shorter faces ($p = 1.08E-8$, $R^2 = 0.61$) and their ears were in a significantly lower position ($p = 3.54E-8$, $R^2 = 0.62$) manifesting a "droopy ear" characteristic. Besides these face alternations, $Tbx15^{-/-}$ mutant mice displayed significantly lower weight as well as shorter body and limb length. $Pax1^{-/-}$ mutant mice showed significantly longer noses ($p = 1.14E-5$, $R^2 = 0.46$) relative to *WT* littermates, but otherwise displayed less obvious morphological alterations than $Tbx15^{-/-}$ mutant mice did. We provide the first direct functional evidence that two well-known and replicated human face genes, *Tbx15* and *Pax1*, impact facial and other body morphology in mice. The general agreement between our

---

Abbreviations: $Pax1^{-/-}$, *Pax1* homozygous mice; $Pax1^{+/-}$, *Pax1* heterozygous mice; $Pax1^{+/+}$, *Pax1* wild-type mice; $Tbx15^{-/-}$, *Tbx15* homozygous mice; $Tbx15^{+/-}$, *Tbx15* heterozygous mice; $Tbx15^{+/+}$, *Tbx15* wild-type mice.

Fan Liu and Lei Liu contributed equally.

findings in knock-out mice with those from previous GWASs suggests that the functional evidence we established here in mice may also be relevant in humans.

KEYWORDS

facial morphology, genetics, genotype, phenotype

1 | INTRODUCTION

Human facial morphology represents a set of highly variable, multidimensional, highly correlated, symmetrical, and strongly heritable complex phenotypes. Unveiling the genetic basis of human facial variation is of fundamental and applied value in developmental biology, evolutionary biology, human genetics, medical genetics, and forensic genetics.

Several independent genome-wide association studies (GWASs) on human facial morphology highlighted DNA variants in or closed to *TBX15* and *PAX1* with genome-wide significant association with human facial phenotypes.[1–7] In particular, Xiong et al. found DNA variants near *TBX15* and *PAX1* significantly associated with human face length and nose width, respectively.[1] Adhikari et al. reported SNPs in *TBX15* to be significantly associated with two human ear traits, folding of the antihelix and antitragus size.[2] Claes et al. and White et al. showed *TBX15* and *PAX1* intron variants to be significantly associated with human facial shape.[3,6] Adhikari et al. and Shaffer et al. reported a significant association of *PAX1* intergenic variants with human nose wing breadth.[4,5]

TBX15 belongs to the T-box family of genes, which encode a phylogenetically conserved family of transcription factors that regulate a variety of developmental processes.[8] *Tbx15* is expressed in limb mesenchymal cells and has a significant function in limb development.[9–11] Genetic variants in *TBX15* result in cousin syndrome, characterized by craniofacial deformity, scapular hypoplasia, pelvic dysplasia, and short stature.[12–14] *PAX1* is a member of the paired box (*PAX*) family of transcription factors and encodes a transcriptional activator which regulates tissue development and cellular differentiation in embryos.[15] *PAX1* mutations cause autosomal recessively inherited otofaciocervical syndrome, characterized by facial dysmorphism and external ear anomalies.[16] *PAX1* acts as an important regulator of chondrocyte maturation.[17] Deletion of the short arm region of chromosome 20 including the *PAX1* gene locus causes craniofacial deformities and abnormal vertebral bodies.[18]

Taking all available genetic knowledge together allows concluding that *TBX15* and *PAX1* play a role in facial morphology in humans. However, direct evidence has been scarce for the functional involvement of these genes in the development and determination of facial morphology.

Although previous in vivo experiments revealed that *Tbx15* acts as an essential effector in the development of the skeleton of the limb, vertebral column, and head[10] and *Tbx15*$^{-/-}$ mutant mice exhibit lower weight, glucose intolerance, and obesity on high-fat diets,[19–21] these studies did not explore the effect of *Tbx15* on facial morphology in mice exhaustively. Moreover, no in vivo functional work has been reported for *Pax1* in mice facial morphology.

In this study, to enhance our functional understanding of the involvement of *Tbx15* and *Pax1* in facial morphology in mice, we, respectively, knocked out these genes by applying the one-step CRISPR/Cas9 method.[22] On mutant and wild-type (*WT*) mice, we acquired 3D images through the HandySCAN BLACK scanner. Based on the collected digital imagery, we quantitatively assessed facial morphology as pairwise Euclidean distances between a set of anatomically meaningful facial landmarks, and also quantified other morphological phenotypes such as weight, body length, fore, and hind limb length. Finally, the morphological differences between mutant mice and *WT* littermates were compared using appropriate statistical tests.

2 | MATERIALS AND METHODS

2.1 | Samples

The mouse strain was C57BL/6J. Amplify Cas9 and sgRNAs, purify them, and use them as a template for in vitro transcription. Fertilized eggs obtained from super-ovulated females (C57BL/6J, 4 weeks) mated with males (C57BL/6J, 7–8 weeks) were microinjected with mixtures of Cas9 mRNA and sgRNA. The injected fertilized eggs were cultured to day 2 and transferred to female mice. Finally, positive mice with a 20 bp frameshift mutation in the second exon of the *Tbx15* gene were obtained. Positive mice with the second exon of the *Pax1* gene completely knocked out were also obtained. The discrimination criterion was the presence of a 20 bp frameshift mutation in the second exon of the *Tbx15* gene and the second exon of the *Pax1* gene. The mice were raised in a pathogen-free environment and bred according to SPF animal breeding standards. The ambient temperature was 20–25°C, and humidity was 40%–70%. The F0 generation-positive

mice were mated with wild-type C57 mice to obtain the heterozygous F1 generation mice. The heterozygous F1 mice were then mated with a female-to-male ratio of 2:1 to produce the homozygous F2 generation mice. After eight months of breeding experiments, we obtained a total of 38 F2 9-weeks adult *Tbx15* mice, that is, 10 homozygous *Tbx15*$^{-/-}$, 18 heterozygous *Tbx15*$^{+/-}$, 10 wild-type *WT*, and 37 F2 9-weeks adult *Pax1* mice, that is, 12 homozygous *Pax1*$^{-/-}$, 15 heterozygous *Pax1*$^{+/-}$, 10 *WT* littermates. Genotypes of all mice were confirmed by PCR amplification and subsequent Sanger sequencing. The use of laboratory animals (SYXK 2019-0022) was licensed by the Beijing Municipal Science and Technology Commission.

2.2 | Genotyping

Mice tail tissue of 0.3 cm^3 was cut into a 1.5 ml centrifuge tube, then added with 98 μl of mouse tail lysate and 2 μl of proteinase K before incubated in a metal bath at 55°C for 30 min for full lysis. After that, the proteinase K was inactivated by placing the tube in a 95°C metal bath for 10 min. The mixture was centrifuged at 12,000 r/min for 5 min, and the supernatant was collected as the DNA template for genotyping. The *Tbx15* and *Pax1* primers with sequences described in Table S2 were used for PCR amplification in a 50 μl of mixture of 25 μL of 2 × Taq Plus Master Mix (Dye Plus), 2 μl of upstream primer (concentration: 10 μM), 2 μl of downstream primer (concentration: 10 μM), 2 μl of DNA template, and 19 μl of ultrapure water. The PCR procedures for both gene fragments were as follows: (1) Denaturation at 94°C for 5 min; (2) Denaturation at 94°C for 30 s; (3) Annealing at 60°C for 30 s; (4) with different extension times for *Tbx15* at 72°C for 2 min, and *Pax1* at 72°C for 75 s; followed by (5) a final extension at 72°C for 7 min, steps (2–4) were repeated 35 times. Electrophoresis was performed on a 2% agarose gel with a voltage of 125 V and a current strength of 400 A for 30 min. The genotypes were identified with gel electrophoresis and Sanger sequencing. The mouse genotype identification kit was purchased from Nanjing Nuoweizan Biotechnology Co., Ltd. The PCR primers were synthesized by Meiji Biotechnology Co., Ltd.

2.3 | Phenotyping

The 9-week-old F2 mice were weighed with an electronic scale and sacrificed by cervical dislocation. The hair of the mice was removed with a razor and Weiting depilatory cream. Prior to phenotyping, depilated mice were kept in an incubator with ice to maintain a good temperature and air humidity to prevent dryness and other reasons from affecting the facial morphology of mice. Phenotyping was

carried out and finished within 1 h after depilation. Mice were fixed on a holder in a way that the jaw is fully exposed and limbs were fixed. Checks were performed to ensure that the mouth was closed and the upper and lower jaws snap tightly; the ears were not sticky and maintained a normal shape. Body length and limb length of the depilated mice were measured with a Chenguang millimeter ruler. The HandySCAN BLACK scanner was used to scan the three-dimensional surface of depilated mice and 3D images were obtained in the *obj* format with a resolution of 0.3 mm and an accuracy level of 0.03 mm. The 3D coordinates of facial landmarks were obtained using the Geomagic Wrap 3D scanning software which is independent of the manufacturers. Landmark positions were visually examined and images with abnormal landmarks were rescanned.

2.4 | Protein sequence analysis

The *Tbx15* and *Pax1* protein sequences were obtained from the UniProt database.[23,24] Multiple alignments of amino acid sequences were performed using the DNAMAN software. The analysis of the protein conserved domains was performed using the PfamScan software.[25]

2.5 | Statistical analyses

We targeted 17 anatomically meaningful facial landmarks, among which, 9 were homologous of the 13 human facial landmarks as described in the previous face GWAS by Xiong et al.[1] The remaining eight were all on the mouse ears, and there were no corresponding landmarks in previous GWASs of the human face and ear morphology. A generalized Procrustes analysis (GPA) was used to remove affine variations due to shifting, rotation, and scaling. After GPA, a total of 136 Euclidean distances between all pairs of the landmarks and the centroid size were derived. A principal component analysis (PCA) was carried out using the 136 inter-landmark distances as the input. Linear regressions were used to test the genetic association considering the genotype as the explanatory variable, the phenotype as the dependent variable, and sex as the covariate, testing for an additive allele effect, that is, the phenotypic change due to each additional mutant allele. Non-parametric Mann–Whitney U test was used for comparing phenotype PCs and the centroid size between different genotype groups. Unsupervised K-means clustering was used for clustering different genotype groups. Multiple testing was corrected using Bonferroni correction of the effective number of independent phenotypes, which was estimated using the Matrix Spectral Decomposition (matSpD) method.[26] All statistical analyses were conducted using R version 3.5.1 unless otherwise specified.

3 | RESULTS

The sgRNA sequences, the primer sequences, and the characteristics of 75 mice are detailed in supplementary tables (Table S1–S3). Gene knockout strategy, PCR, and Sanger sequencing results for genotyping are detailed in Figure 1. The birth rate of $Tbx15^{-/-}$ mice was significantly lower than WT littermates during a 6-month period (mean birth rate 0.26 vs. 0.74, $p = 0.04$, Figure S1A,B), suggesting an important role of $Tbx15$ in embryonic development. The birth rate of $Pax1^{-/-}$ mice was also lower than that of WT littermates, but not statistically significantly so (Figure S1C,D). In all WT littermates, the facial phenotypes were largely normally distributed (Table S4), and no general differences between males and females were observed (Table S5). As expected, symmetric facial phenotypes showed higher correlations than non-symmetric ones (Table S6), further supporting the reliability of the obtained phenotype dataset. Raw landmark coordinates from all mice showed systematic differences in position, orientation, and scaling (Figure 2A, Figure S2A). They were superimposed onto a consensus 3D Euclidean space based on GPA (Figure 2B, Figure S2B).
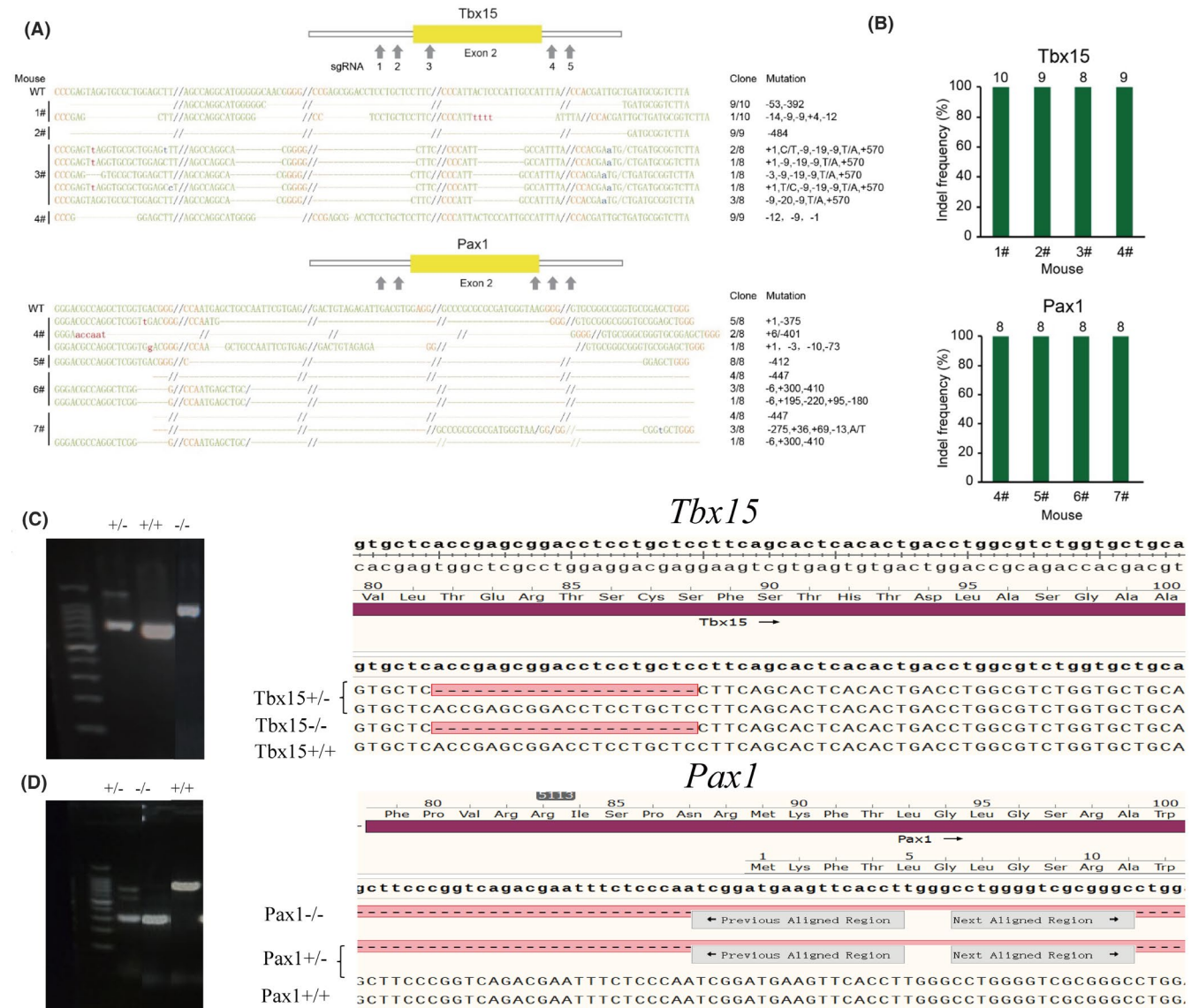

FIGURE 1 Complete deletion of $Tbx15$ and $Pax1$ in mice by CRISPR/Cas9. (A) Clones from the tail were sequenced and analyzed. Schematic of sgRNA-targeting sites in $Tbx15$ and $Pax1$ gene. The sgRNA target sequences and PAM sequences are labeled in green and red, respectively. Hyphens represent deleted nucleotides and omitted regions are indicated by dash lines. (B) The indel frequencies show that $Tbx15$ and $Pax1$ were mutated completely in all mice. The number of clones is denoted above the column. (C) Genotype identification for $Tbx15$ mice by PCR and Sanger sequencing. (D) Genotype identification for $Pax1$ mice by PCR and Sanger sequencing

FIGURE 2 Example of mice image. (A) Landmarks pattern in 2D mice image. (B) Landmarks pattern in 3D mice image. (C) 2D image of *Tbx15* mice. (D) 2D image of *Pax1* mice
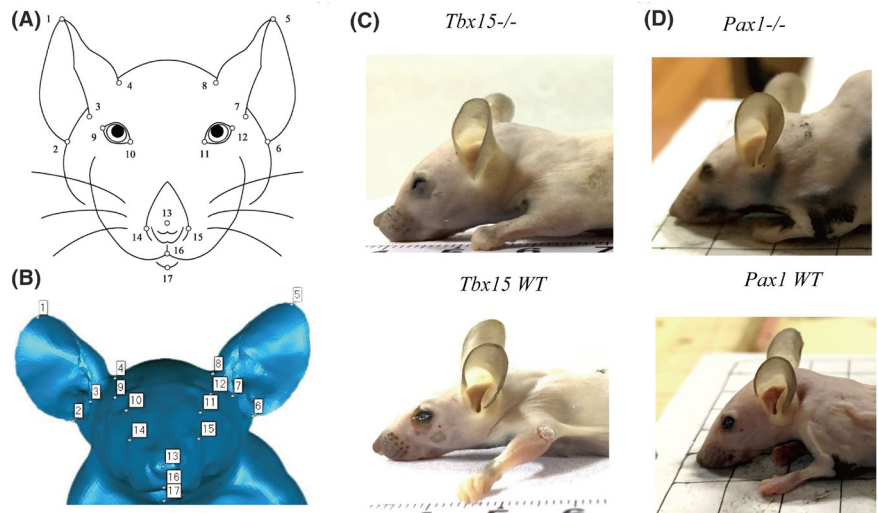

FIGURE 3 Comparison of mice facial morphology with humans. (A) The effect of *Tbx15* on human facial morphology.[6] (B) The effect of *Pax1* on human facial morphology.[5] (C) The effect of *Tbx15 and Pax1* on human facial morphology.[1] (D) The effect of *Tbx15* on mice facial morphology. (E) The effect of *Pax1* on mice facial morphology
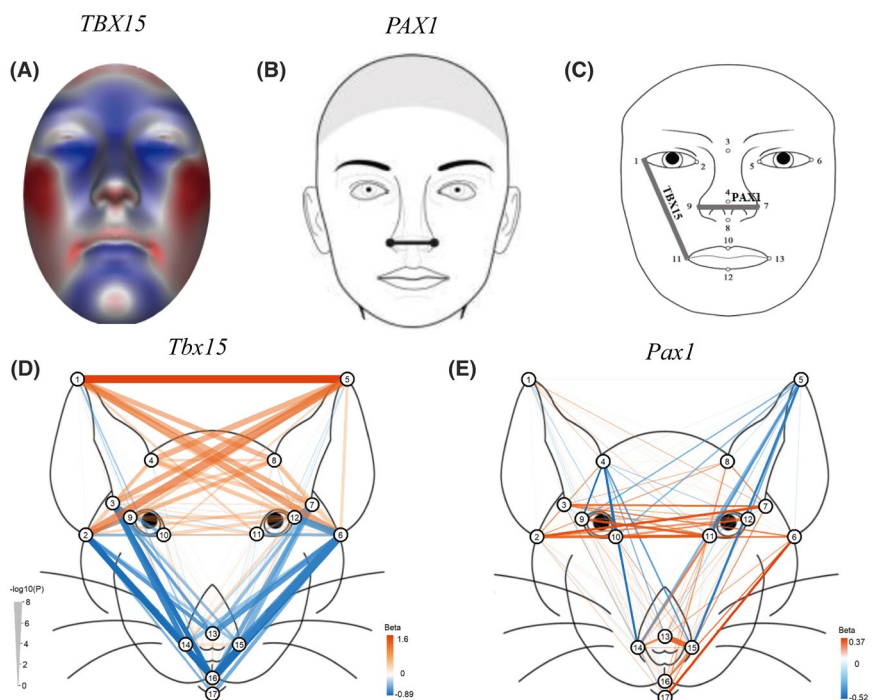
3.1 | Differences in facial phenotypes between mutant and wild-type mice

In the 38 *Tbx15* mice, that is, 10 homozygous $Tbx15^{-/-}$, 18 heterozygous $Tbx15^{+/-}$, 10 WT $Tbx15^{+/+}$, the *Tbx15* genotype was significantly associated with a total of 34 facial phenotypes derived from GPA-transformed landmarks (Bonferroni adjusted $p < 0.05$). Compared with their WT counterparts, the $Tbx15^{-/-}$ mutant mice had significantly shorter faces, which affected 22 phenotypes as characterized by shorter distances between ear root and nose, mouth landmarks, and their ears had a significantly lower position, manifesting a "droopy ear" characteristic. (12 phenotypes, including L1–L8, Figures 2C and 3D, Table S7). The most significant face shortening effect in the *Tbx15* mutant mice was observed for L6–L15 (ear–nose length),

for which the *Tbx15* genotype accounted for 61% of the phenotype variance (0.64 mm per mutant allele). The most significant effect on the ear was observed for L2–L5 (0.95 mm per mutant gene, Figure 3D, Table S7). A PCA analysis of all 136 facial phenotypes resulted in a total of 136 PCs. The top two PCs explained 49.73% of the total phenotype variance. An unsupervised clustering analysis of the top two PCs could completely separate $Tbx15^{-/-}$ and WT littermates (Figure 4A). A Mann–Whitney test of PC1 also showed significant differences between $Tbx15^{+/-}$ and the WT ($p < 0.001$) as well as between $Tbx15^{+/-}$ and $Tbx15^{-/-}$ ($p < 0.001$, Figure 4B), although the centroid size was not significantly different between WT and $Tbx15^{-/-}$ (Figure S3A). These results overall demonstrated significant facial differences between $Tbx15^{-/-}$, $Tbx15^{+/-}$ and WT. Repeating the association analysis using the
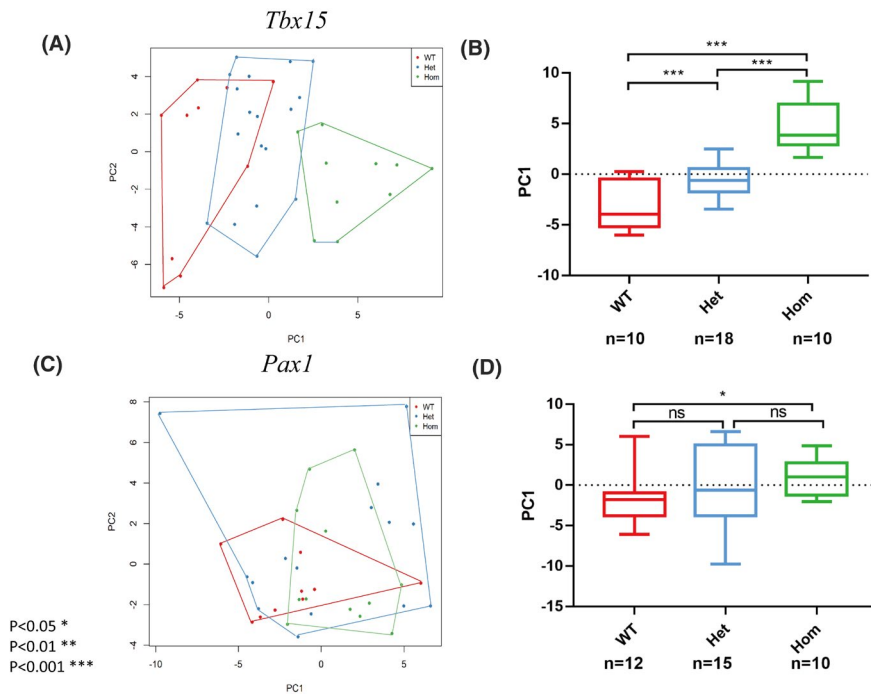
FIGURE 4 Genotypes classification based on principal components (PCs) of 136 facial distances. (A) Genotypes classification in *Tbx15* mice. (B) PC1 differences between *Tbx15* groups. (C) Genotypes classification in *Pax1* mice. (D) PC1 differences between *Pax1* groups

original landmarks before GPA also revealed highly significant differences between *Tbx15* genotype groups for 35 facial phenotypes (Figure S4A).

In the 37 *Pax1* mice, that is, 12 homozygous $Pax1^{-/-}$, 15 heterozygous $Pax1^{+/-}$, 10 *WT* littermates $Pax1^{+/+}$, the *Pax1* genotype was significantly associated with facial variation for only one phenotype after Bonferroni correction (adjusted $p < 0.05$). Compared with the *WT* littermates, the nose length of the $Pax1^{-/-}$ mutant mice was significantly increased (L13–L15, Figures 2D and 3E, Table S8). The *Pax1* genotype explained 46% of the phenotype variance in the *Pax1* mutant mice (0.28 mm per mutant gene). The clustering analysis of the major PCs could not separate *WT*, $Pax1^{+/-}$, and $Pax1^{-/-}$ groups. However, the Mann–Whitney test of the PC1 showed a significant difference between the *WT* and $Pax1^{-/-}$ groups (Figure 4C,D). Centroid size was not significantly different between any *Pax1* genotype groups (Figure S3B). Repeating the association analysis using the original landmarks before GPA also revealed significant differences between *Pax1* genotype groups for three facial phenotypes (Figure S4B).

3.2 | Consistency with previous facial variation GWAS in humans

For both genes, the trends of the facial differences observed between mutant and *WT* littermates were largely consistent with the genetic association effects observed in previous human GWASs (Figure 3).[1–6,27] In particular, *TBX15* variants previously showed a significant association effect on multiple facial phenotypes in humans (Figure 3A)[6] and

Tbx15 mutant mice had shorter faces as demonstrated here. The droopy ear characteristic, however, which we observed in *Tbx15* mutant mice had no strict correspondence with findings in previous human GWASs, although Adhikari et al. reported *Tbx15* variants associated with ear helix rolling and antihelix.[2] Interestingly, Xiong et al. found that SNPs at *Tbx15* had asymmetrical effects on human facial morphology (Figure 3C).[1] In our in vivo mice experiments, $Tbx15^{-/-}$ mice showed highly symmetrical effects on decreasing ear–mouth distances (1.00E-8 $< p <$ 1.66E-4, Figures 2C and 3D, Table S7). The failure of observing an asymmetric effect of *Tbx15* in our experiments might be explained by a pronounced effect of gene silencing compared with the potential regulatory effects of the SNPs. For *Pax1*, previous GWASs on facial shape in humans mainly found effects on nose width (Figure 3B,C).[1,4,5] In our experimental mice study, although no direct changes in nose width (L14–L15) were observed in $Pax1^{-/-}$ mice, we found that *Pax1* mutant mice had a significantly increased nose length (L13–L15) which is partly a representation of nose width (L14–L15, Figure 2D, Figure 3E, Table S8). No direct changes in nose width were observed in mice, probably due to insufficient sample size and facial structure differences between mice and humans.

3.3 | Differences in other physical phenotypes between mutant and wild-type mice

Next to the effects of *Tbx15* and *Pax1* gene editing on facial phenotypes in mice, we additionally investigated the effects

on other physical morphological phenotypes such as body weight, body length, and length of fore and hind limbs. Compared with *WT* littermates, *Tbx15*$^{-/-}$ mice had significantly lower body weight ($p < 0.01$), shorter body length ($p < 0.001$), and shorter limb length ($p < 0.01$, Figure 5). For *Pax1*, the body weight, body length, limb length of the mutant mice were also reduced compared to *WT* littermates, but not statistically significantly so (Figure S5).

## 3.4 | Protein sequence conservation between mice and humans

The *Tbx15* protein sequences are composed of 602 amino acid sequences in both humans and mice. An amino acid sequence alignment analysis revealed that the amino acid sequences in both species had a very high identity (98.67%) and the same very long conserved T-box domain was found in humans and mice. The high level of evolutionary conservation between mice and humans, together with the significantly lower birth rate of *Tbx15*$^{-/-}$ in mice, confirms an important role of *Tbx15* in the early development of embryogenesis, both in humans and in mice.

The *Pax1* protein is composed of 534 amino acids sequence in mice and 446 amino acids in humans with a relatively high level of identity (73.41%), but considerably lower than seen for *Tbx15*. Furthermore, the two species shared a common set of domains in *Pax1*, including a "Paired box" domain, a homeodomain-like domain, and a winged helix-turn-helix conserved domain. The relatively high sequence conservation may suggest a vital role of *Pax1* in the early development of embryogenesis in both species.

4 | DISCUSSION

Our in vivo gene editing experiments in mice for two well-replicated human face *Tbx15* and *Pax1* genes provide novel evidence on the functional involvement of these two genes in facial and other physical morphology in mice, at least. The general agreement between our findings in knock-out mice with those from previous GWASs suggests that the functional evidence we established here in mice may also be relevant in humans, which is of value in developmental biology, evolutionary biology, human genetics, medical genetics, and forensic genetics.

Tbx15$^{-/-}$ mice showed a shortened facial length and manifesting a droopy ear characteristic. In addition, they showed reduced weight, shortened body and limb length which is consistent with the findings from a previous mice study.[20] The *TBX15* gene plays a major role in the development of the mesoderm of all vertebrates.[28] The complete inactivation of the mouse *Tbx15* in mice and *TBX15* mutations in humans lead to severe bone deformities.[10,13,29] Notably, previous literature also showed that *Tbx15* affects the development of the skeleton of the limb, vertebral column, head, limbs, vertebrae, and ribs by controlling the number of mesenchymal precursor cells and cartilage cells,[10,14] while the *Tbx15* effect on the face in mice was few studied before. Our new findings together with previous ones support our conclusion, that *Tbx15* plays an important role in the development of facial and limb morphology in mice. Because the facial shape effects we observed in the *Tbx15*$^{-/-}$ mutant mice are largely in line with the *Tbx15* association effects in humans previously reported in different GWASs, we suggest that the
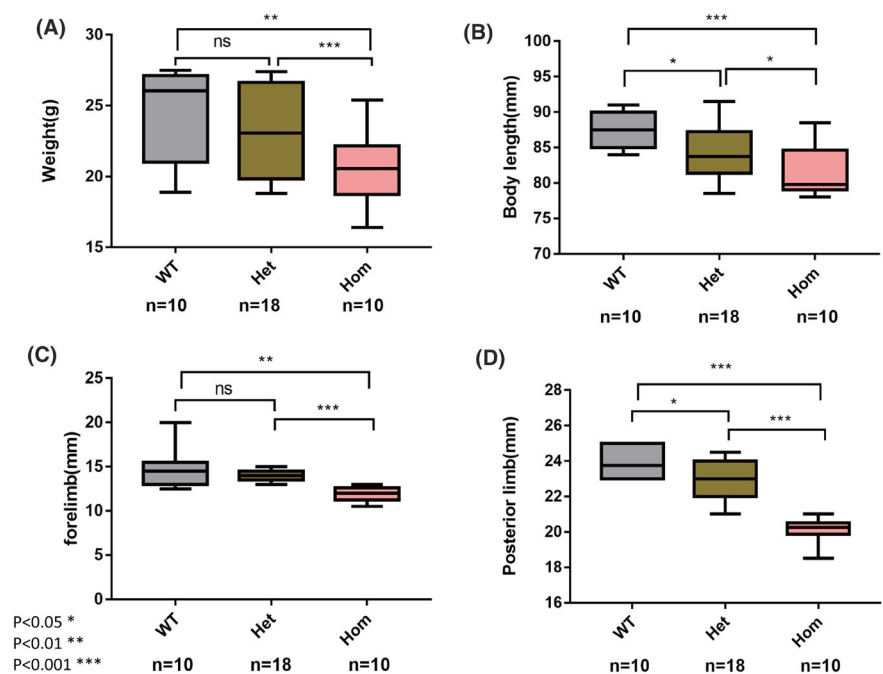
FIGURE 5 Effects of *Tbx15* on mice weight, body length, fore, and hind limb length. (A) Weight. (B) Body length. (C) Forelimb length. (D) Posterior limb length

functional impact of *Tbx15* on the facial shape we revealed here in mice also exists in humans, which needs to be confirmed by future work.

Moreover, *Pax1*$^{-/-}$ mice showed an increased nose length in our study. Earlier studies revealed that *Pax1* is a key transcription factor affecting cartilage development and regulates the expression of cartilage-related genes in the early stages of development.[17] Meanwhile, previous studies of the *Pax1/Pax9* multiple allele KO mutants uncovered their synergistic roles in axial skeleton development, demonstrating a clear gene-dosage effect of *Pax9* in the absence of *Pax1*, with increasing severity of the vertebral column malformations, whereby *Pax1*$^{-/-}$*Pax9*$^{-/-}$ mutants exhibit a complete loss of vertebral bodies and intervertebral discs, deformed proximal parts of the ribs and a lack of caudal vertebrae.[30,31] *Pax1*$^{-/-}$exhibit variably severe morphological alterations of the vertebral column, sternum, scapula, skull, and thymus, with reduced adult survival and fertility and some heterozygotes show milder skeletal abnormalities.[32–34] In our study of *Pax1*$^{-/-}$ mice, these phenotypes appeared much weaker from surface appearance. Only one out of 10 *Pax1*$^{-/-}$ mice manifested obvious deformation of coccyx (Figure S6). However, the observation of weaker phenotypes from the surface appearance is not in conflict with previous studies which used micro-CT images for capturing subtle variation in the skeleton. Since the nasal bone contains a cartilage component, our findings of *Pax1* determining nose morphology in mice may be explained by its effect on the development of nose cartilage, which needs to be further explored. We did observe reduced body weight, body length, and limb length in the *Pax1*$^{-/-}$ mice compared to *WT* littermates, but the effect was not statistically significant, may be because of small effect and thus insufficient sample size. Although the facial shape effects we observed in the *Pax1*$^{-/-}$ mutant mice are not fully consistent with *Pax1* associations effects in humans previously reported in different GWASs, as in humans *Pax1* associations were seen with nose width, while our in vivo data show that *Pax1* affects nose length in mice, in both species this gene is involved in nose-related phenotypes. Therefore, we suggest that the functional effect of *Pax1* on the facial shape we revealed here in mice is similar to the effect of *Pax1* in humans, which also needs to be confirmed by future work.

Our approach has several advantages. We selected the 9-week-old F2 generation mice because nine weeks is an acceptable time point for adult-like craniofacial form in mice and their skeletal is matured in this time.[35] Furthermore, we selected littermate mice of different genotypes for phenotype observation and our littermate-born design prevented potential noises

caused by unobserved environmental factors. Moreover, the inclusion of the heterozygote mice in the analysis further expanded the sample size and was helpful in observing potential trend effects. In addition, compared to previous phenotyping methods, our phenotyping method focusing on 3D surface appearance may have certain advantages. For example, Kaustubh et al. analyzed the effect of *EDAR* on ear morphology in mice by taking 2D photographs of superior and lateral views of the head and then acquired 2D coordinates for morphological analysis.[2] Compared to 2D landmarks, 3D landmarks are more robust against shifting, rotation, and scaling. Compared with the studies using micro-CT images, 3D surface images may capture additional information from facial soft tissue thickness.[7]

In conclusion, we provide the direct functional evidence that two well-known and replicated human face genes, *Tbx15* and *Pax1*, impact facial and other body morphology in mice. *Tbx15* seems to affect the face globally, while *Pax1* is mainly affecting the nose, with such a pattern being similar in both mice and humans. In future research studies, functional effects of other human face genes highlighted in previous GWASs should be investigated to take our increasing knowledge on human face genetics from the statistical associational level to the next level of functional proof.

CONFLICT OF INTEREST
The authors declare that no conflicts of interest exist.

AUTHOR CONTRIBUTIONS
FL and LL conceived the study and provided most of the resources; YQ and YL conducted genotyping experiments and obtained the genotypic data. YQ and ZX obtained phenotypic data and conducted statistical analyses; YQ, FL, and MK wrote the manuscript; all authors commented on the manuscript and approved the final version prior to submission.

ETHICS APPROVAL
The use of laboratory animals (SYXK 2019-0022) was licensed by the Beijing Municipal Science and Technology Commission.

REFERENCES

1. Xiong Z, Dankova G, Howe LJ, et al.; International Visible Trait Genetics (VisiGen) Consortium. Novel genetic loci affecting facial shape variation in humans. *Elife*. 2019;8:e49898.
2. Adhikari K, Reales G, Smith AJ, et al. A genome-wide association study identifies multiple loci for variation in human ear morphology. *Nat Commun*. 2015;6:7500.
3. Claes P, Roosenboom J, White JD, et al. Genome-wide mapping of global-to-local genetic effects on human facial shape. *Nat Genet*. 2018;50:414-423.
4. Adhikari K, Fuentes-Guajardo M, Quinto-Sanchez M, et al. A genome-wide association scan implicates DCHS2, RUNX2, GLI3, PAX1 and EDAR in human facial variation. *Nat Commun*. 2016;7:11616.
5. Shaffer JR, Orlova E, Lee MK, et al. Genome-wide association study reveals multiple loci influencing normal human facial morphology. *PLoS Genet*. 2016;12:e1006149.
6. White JD, Indencleef K, Naqvi S, et al. Insights into the genetic architecture of the human face. *Nat Genet*. 2020;53(1):45-53.
7. Bonfante B, Faux P, Navarro N, et al. A GWAS in Latin Americans identifies novel face shape loci, implicating VPS13B and a denisovan introgressed region in facial variation. *Science advances*. 2021;7:eabc6160.
8. Castellanos R, Xie Q, Zheng D, Cvekl A, Morrow BE. Mammalian TBX1 preferentially binds and regulates downstream targets via a tandem T-site repeat. *PLoS One*. 2014;9:e95151.
9. Farin HF, Mansouri A, Petry M, Kispert A. T-box protein Tbx18 interacts with the paired box protein Pax3 in the development of the paraxial mesoderm. *J Biol Chem*. 2008;283:25372-25380.
10. Singh MK, Petry M, Haenig B, Lescher B, Leitges M, Kispert A. The T-box transcription factor Tbx15 is required for skeletal development. *Mech Dev*. 2005;122:131-144.
11. Tanaka M, Tickle C. Tbx18 and boundary formation in chick somite and wing development. *Dev Biol*. 2004;268:470-480.
12. Dikoglu E, Simsek-Kiper PO, Utine GE, et al. Homozygosity for a novel truncating mutation confirms TBX15 deficiency as the cause of cousin syndrome. *Am J Med Genet A*. 2013;161A:3161-3165.
13. Lausch E, Hermanns P, Farin HF, et al. TBX15 mutations cause craniofacial dysmorphism, hypoplasia of scapula and pelvis, and short stature in Cousin syndrome. *Am J Hum Genet*. 2008;83:649-655.
14. Kuijper S, Beverdam A, Kroon C, et al. Genetics of shoulder girdle formation: roles of Tbx15 and aristaless-like genes. *Development*. 2005;132:1601-1610.
15. Robson EJ, He SJ, Eccles MR. A PANorama of PAX genes in cancer and development. *Nat Rev Cancer*. 2006;6:52-62.
16. Pohl E, Aykut A, Beleggia F, et al. A hypofunctional PAX1 mutation causes autosomal recessively inherited otofaciocervical syndrome. *Hum Genet*. 2013;132:1311-1320.
17. Takimoto A, Mohri H, Kokubu C, Hiraki Y, Shukunami C. Pax1 acts as a negative regulator of chondrocyte maturation. *Exp Cell Res*. 2013;319:3128-3139.
18. Receveur A, Brisset S, Martinovic J, et al. Prenatal diagnosis of isochromosome 20q in a fetus with vertebral anomaly and rocker-bottom feet. *Taiwan J Obstet Gynecol*. 2017;56:677-680.
19. Sun W, Zhao X, Wang Z, et al. Tbx15 is required for adipocyte browning induced by adrenergic signaling pathway. *Molecular metabolism*. 2019;28:48-57.
20. Lee KY, Singh MK, Ussar S, et al. Tbx15 controls skeletal muscle fibre-type determination and muscle metabolism. *Nat Commun*. 2015;6:8054.
21. Lee KY, Sharma R, Gase G, Ussar S. Tbx15 defines a glycolytic subpopulation and white adipocyte heterogeneity. *Diabetes*. 2017;66:2822-2829.
22. Zuo E, Cai YJ, Li K, et al. One-step generation of complete gene knockout mice and monkeys by CRISPR/Cas9-mediated gene editing with multiple sgRNAs. *Cell Res*. 2017;27:933-945.
23. The UniProt C. UniProt: the universal protein knowledgebase. *Nucleic Acids Res*. 2017;45:D158-D169.
24. UniProt C. UniProt: a hub for protein information. *Nucleic Acids Res*. 2015;43:D204-212.
25. Mistry J, Bateman A, Finn RD. Predicting active site residue annotations in the Pfam database. *BMC Bioinformatics*. 2007;8:298.
26. Li J, Ji L. Adjusting multiple testing in multilocus analyses using the eigenvalues of a correlation matrix. *Heredity*. 2005;95:221-227.
27. Gao C, Langefeld CD, Ziegler JT, et al. Genome-wide study of subcutaneous and visceral adipose tissue reveals novel sex-specific adiposity loci in Mexican Americans. *Obesity*. 2018;26:202-212.
28. Herrmann BG, Labeit S, Poustka A, King TR, Lehrach H. Cloning of the T gene required in mesoderm formation in the mouse. *Nature*. 1990;343:617-622.
29. Candille SI, Van Raamsdonk CD, Chen C, et al. Dorsoventral patterning of the mouse coat by Tbx15. *PLoS Biol*. 2004;2:E3.
30. Wallin J, Wilting J, Koseki H, Fritsch R, Christ B, Balling R. The role of Pax-1 in axial skeleton development. *Development*. 1994;120:1109-1121.
31. Wilm B, Dahl E, Peters H, Balling R, Imai K. Targeted disruption of Pax1 defines its null phenotype and proves haploinsufficiency. *Proc Natl Acad Sci USA*. 1998;95:8692-8697.
32. Bult CJ, Blake JA, Smith CL, et al. Mouse Genome Database (MGD) 2019. *Nucleic Acids Res*. 2019;47:D801-D806.
33. Smith CM, Hayamizu TF, Finger JH, et al. The mouse Gene Expression Database (GXD): 2019 update. *Nucleic Acids Res*. 2019;47:D774-D779.
34. Krupke DM, Begley DA, Sundberg JP, Richardson JE, Neuhauser SB, Bult CJ. The mouse tumor biology database: a comprehensive resource for mouse models of human cancer. *Can Res*. 2017;77:e67-e70.
35. Maga AM. Postnatal development of the craniofacial skeleton in male C57BL/6J mice. *J Am Assoc Lab Anim Sci*. 2016;55:131-136.

SUPPORTING INFORMATION

Additional supporting information may be found online in the Supporting Information section.